Author version: *Mar. Pet. Geol., vol.64; 2015; 324-333*

Formation of methane-related authigenic carbonates in a highly dynamic biogeochemical system in the Krishna-Godavari Basin, Bay of Bengal

M. Kocherla[1]*, B.M.A. Teichert[2], S. Pillai[1], M. Satyanarayanan[3], P.B. Ramamurthy[3], D.J. Patil[3], A.N. Rao[4]

[1]CSIR-National Institute of Oceanography, Dona Paula, Goa, 403004, India
[2]Institut für Geologie und Paläontologie, Westfälische Wilhelms-Universität Münster, Corrensstr. 24, 48149 Münster, Germany
[3]CSIR-National Geophysical Research Institute, Uppal Road, Hyderabad-500606, India.
[4]Department of Geology, Osmania University, Hyderabad-500007 India.

*Corresponding author email: kocherla@nio.org

Abstract

We report the abundant occurrence of authigenic Fe-rich carbonate, high Mg-calcite (HMC) and low Mg-calcite from 11 cores recovered from the Krishna-Godavari Basin (K-G Basin), Bay of Bengal. The cores were collected as part of the Indian gas hydrate exploration program on board R/V *Marion Dufresne* (MD-161: May, 2007) in different environments, including mounds (mud diapirs), mass flows, and hemipelagic sediments over a range of water depths from 647 to 2,079 m. Authigenic carbonates range in size from 1 mm to 12 cm and display various morphologies like roundish or platy (micro-) nodules and tube-like forms. From the cores, 173 carbonate samples have been investigated for their depth distribution, mineralogy, geochemical and stable isotopic composition. The stable carbon isotopic composition of 46 out of 88 measured carbonate samples are around -50 ‰ which allows the differentiation into methane-related carbonates (HMC), especially at Sites 8 and 15, but also in low abundance at Sites 1, 5, 9 and 12. Results indicate that the carbonates at Site 8 and 15 represent paleo methane seepage locations. The Fe-rich carbonates occur abundantly at many sites in the K-G Basin. Their varying carbon isotopic composition indicates that probably not only sulfate reduction through organic matter degradation but also methanogenesis are the responsible processes for their formation.

Keywords: Authigenic carbonates; Krishna-Godavari offshore basin; Bay of Bengal; stable carbon isotopes, stable oxygen isotopes.

1. Introduction

Methane-derived authigenic carbonates are witnesses of diffuse to vigorous, focused methane flux in regions where also gas hydrates often occur (e.g. Han and Suess, 1989; Hovland et al., 1987; Mazzini et al., 2006; Teichert et al., 2005a; von Rad et al., 1996). These authigenic carbonates occur in many different morphologies like slabs, nodules, pavements, build-ups, chemoherms, bioturbation casts, and tubes or as dispersed crystals ranging in size from millimetre to tens of meters. The precipitation of authigenic carbonates is mainly linked to the microbial reduction of sulphate either via organic matter (equation 1) or anaerobic methane oxidation (equation 2).

$$2CH_2O + SO_4^{2-} \Longleftrightarrow 2HCO_3^- + H_2S \quad (1)$$

$$CH_4 + SO_4^{2-} \Longleftrightarrow HCO_3^- + HS^- + H_2O \quad (2)$$

During both biogeochemical processes bicarbonate [HCO_3^-] is being produced and thus pore water alkalinity increases. This will lead together with seawater calcium to the precipitation of authigenic carbonate minerals (equation 3).

$$Ca^{2+} + 2HCO_3^- \Longleftrightarrow CaCO_3 + CO_2 + H_2O \quad (3)$$

It is important to determine which of the above processes (equation 1 and 2) are responsible for authigenic carbonate formation because the process reveals valuable information about the biogeochemical environment of carbonate formation and possibly advection of methane-rich fluids. Since authigenic carbonates are not only witnesses of ongoing methane seepage but also paleo seepage activity, they are usually the only remnants with which paleo methane seepage can be reconstructed (Mazumdar et al., 2009; Peckmann et al., 2009; Teichert et al., 2003). In addition, the morphologies of the authigenic carbonates can give an indication about the relative fluid flux rate. Focused fluid flow will rather lead to carbonate build-ups like chemoherms while diffusive fluid flow leads to disseminated carbonate cements and finally carbonate pavements (e.g. Naehr et al., 2007; Suess, 2014; Teichert et al., 2005b).

In the northern Indian Ocean, occurrences of methane-derived authigenic carbonates are reported from the Krishna-Godavari (K-G) Basin along the Eastern Continental Margins of India (ECMI) (Kocherla et., al., 2006; Mazumdar et al., 2009) and from the Makran accretionary prism off Pakistan in the Arabian Sea (von Rad et al., 1996; von Rad et al., 2000; Klauda and Sandler, 2005). The continental slope region of the K-G Basin is one of the promising petroliferous basins of India and the recent drilling and coring carried out during the National Gas Hydrate Program Expedition 01 (NGHP-01) in 2006 (Collett et al., 2008) confirmed the presence of massive authigenic carbonate precipitates (Teichert et al., 2014) along with more than 100 m thick accumulation of gas

hydrates in the K-G Basin (Collett et al., 2008, 2014; Dewangan et al., 2010; Kumar et al., 2014; Ramana et al., 2007, 2009).

During the R/V *Marion Dufresne* cruise (MD-161, May 2007) 17 sediment cores of various lengths (25-35 m long) were recovered from geological settings, including mud diapirs, mass flows, and hemipelagic sediments over a range of water depths (647-2,079 m) in the K-G Basin (Table 1). This cruise was part of the gas hydrate research program at the National Institute of Oceanography, Goa, with the objective to characterise sediments and diagenetic minerals with respect to their value as recorders of methane-rich fluid advection and accompanying gas hydrate formation. In this study, we present a unique data set from 11 cores in the K-G Basin that provide a deep insight into the history of biogeochemical processes within the sediments. The proximity of the cores records the high variability of different processes within short distances.

2. Geological setting

The study area in the K-G Basin lies in the middle of Eastern continental Margins of India (ECMI) which is a pericratonic rift basin (Rao, 2001) that evolved after the breakup of Gondwanaland around 130 Ma years ago (Powell et al., 1988; Scotese et al., 1988; Ramana et al., 1994). Onshore extension of K-G Basin is ~28,000 km^2 and its offshore extension is ~145,000 km^2 (Ojha and Dubey, 2006). Much of the detrital influx into the K-G Basin is brought by the two major river systems: Krishna and Godavari Rivers. The sediment thickness ranges from 3-5 km in onshore region to ~8 km in the offshore portion of the basin (Prabhakar and Zutshi, 1993; Basti, 2007) with several cycles of deposition, ranging in age from late Carboniferous to Pleistocene. The sediment in the study area consists of silty clay with negligible amount of sand (Kocherla et al., 2006). The dominant clay fraction is smectite with low abundances of illite and kaolinite and very little chlorite (Phillips et al., 2014).

In the K-G Basin, widespread presence of gas hydrate is manifested in the multi-channel seismic data in the form of bottom simulating reflectors (BSRs). Drilling and coring in the K-G Basin has confirmed the presence of gas hydrate (Collett et al., 2008). Several acoustic features related to fluid and/or gas migration have been reported in the shallow subsurface (Dewangan et al., 2010; Ramana et al., 2007, 2009) suggesting active migration of methane in the study area. The geological and geochemical analyses of long sediment cores, acquired on-board the R/V *Marion Dufresne*, have confirmed paleo-methane seepage in the study area (Mazumdar et al., 2009). Slumping/sliding of slope sediments, associated with fluid and/or gas migration, has led to mass transport deposits in the K-G offshore basin (Ramprasad et al., 2011). Several bathymetric mounds formed due to shale tectonics are heavily faulted and show acoustic signatures of fluid and/or gas migration through the fault system (Dewangan et al., 2010). The analysis of available geophysical datasets such as multi-channel seismic, high resolution seismic, sub-bottom profiler, and multibeam

bathymetry has divided the study area into distinct depositional environments, including mid-slope mini basins, in the north-east and south-west directions, bathymetric mounds, toe-thrust sedimentary ridges, and deep oceanic basin (Dewangan et al., 2010; Ramana et al., 2007, 2009; Ramprasad et al., 2011).

Total organic carbon (TOC) content of the sediments in the K-G basin is mainly from terrestrial sources supplied by the Krishna and Godavari rivers. The terrestrial source is also indicated by studies on the provenance of the sediments with the main source being the Deccan basalts (Phillips et al., 2014). The high terrestrial fluxes and sedimentation rates and the consequently rapid burial have resulted in a high preservation of TOC in the K-G basin sediments (Johnson et al., 2014).

3. Samples and methods

A total of 11 long cores with lengths between 20 and 34 m were recovered over a water depth range of 790 to 2079 m (Table 1, Fig. 1). The cores were retrieved during R/V *Marion Dufresne* cruise (MD-161, May 2007) in the K-G Basin using a Giant Calypso piston corer. On-board analysis of sediment cores revealed that the main lithology is nannofossil-bearing clay with silty beds with a high terrigenous organic carbon content. A total of 173 authigenic carbonates were subsampled from the sediment cores (Table 2). The shallowest carbonate sample is from 3.4 mbsf (meters below seafloor) and the deepest is from 29 mbsf (Fig. 2). The authigenic carbonate show different colors from greyish, to yellowish and brownish shadings. They are either semi-lithified or hard and completely lithified. The morphologies are variable (Fig. 3). Roundish or platy nodules (0.1 - 12 cm) or micro-nodules (<0.1 cm) are very common followed by tube-like forms (Fig. 3). Samples were washed with water to remove the salts and then washed in an ultrasonic bath for 15 minutes. Finally they were dried and powdered with an agate mortar and pestle for further analyses.

Bulk mineralogy of all carbonate precipitates was determined by X-ray diffraction (XRD) on randomly oriented samples using a Regaku X-ray diffractometer (Ultima-IV). All samples were run from 25 to 35 °2θ at 1°/min scan speed using CuKα radiation (λ = 1.541838Å) at the National Institute of Oceanography, Goa, India. The shift in the d_{104} calcite peak was used to determine the Mg content of calcite and dolomite (Lumsden, 1979). For the Fe-rich carbonates, we cannot exclude the incorporation of other cations like Ca^{2+}, Mg^{2+} and Mn^{2+} into the crystal lattice therefore are not identified as siderites.

Dried and disaggregated unlithified samples as well as freshly broken surfaces of carbonates were first examined under a binocular microscope to select appropriate samples for scanning electron microscope (SEM) analyses to study crystal habits and chemistry using a JEOL-JSM 5800 LV1 equipped with an Energy Dispersive Spectrometer (EDS) at the National Institute of Oceanography, Goa, India.

Inorganic carbon (IC) content of 92 carbonate precipitates was determined using a CO_2 coulometer of UIC (CM Model 5130). About 30 mg of freeze-dried, ground sediment are acidified with 2N HCl in a heated vial to generate carbon dioxide. Carbon dioxide free air carries the CO_2 through a scrubbing system into the coulometer for detection. In the coulometer cell, the CO_2 is quantitatively absorbed, reacting with monoethanolamine to form a titratable acid that causes the color to fade. Calibration is performed using pure calcium carbonate as a standard. The weight percentage of calcium carbonate (Table 2) is calculated from the IC content, with the assumption that all inorganic carbon is present as calcium carbonate.

Carbon and oxygen isotope ratios of 88 authigenic carbonates were determined with a Thermo Finnegan Delta Plus XP continuous-flow isotope ratio mass spectrometer attached to a Gas Bench II and equipped with a PAL auto sampler at the National Geophysical Research Institute, Hyderabad, India. All values are reported in per mil (‰) relative to VPDB (Vienna Peedee belemnite) standard. A sample reproducibility of 0.1 ‰ for both carbon and oxygen is reported here.

4 Results

4.1 Mineralogy of authigenic carbonates

Bulk mineralogical analyses with XRD reveals three main carbonate mineralogies: low Mg-calcite (LMC, 5-6 Mol% $MgCO_3$), high Mg-calcite (HMC, 10-18 Mol% $MgCO_3$) and Fe-rich carbonates (Table 2). For few samples at Site 15 the low carbonate content prevented a reliable determination of carbonate mineralogy. These samples are therefore referred to as calcite. A general observation is that the HMC samples are mostly gray in color and lithified while the Fe-rich carbonates are mostly brownish and semi-lithified. Minor mineralogies that were identified by XRD are strontianite, witherite, rhodochrosite, cerussite, aragonite, barite and pyrite. At Sites 8 and 15, high Mg-calcite is the dominating mineralogy with only few calcitic and LMC samples. HMC occurs only at Sites 1 and 5 as single samples and at Site 9 as a single sample of LMC. SEM analyses reveals porous structures in the Fe-rich carbonates, similar to (gas?) vesicles (Fig. 4). An euhedral microcrystalline structure is typical for these carbonates. The $CaCO_3$ content (wt %) of the authigenic carbonates ranges from 10 to 81 % (Table 2).

4.2 Stable isotopic compositions of authigenic carbonates

The Fe-rich carbonates show the widest range in oxygen and carbon isotopic composition ranging from 0.1 to 6.1 ‰ and -35.4 to +6.4 ‰, respectively (Table 2, Fig. 5). The HMC reveals more restricted values especially for carbon isotopes with $\delta^{18}O$ and $\delta^{13}C$ values ranging from 0.3 to 5.4 and -27.8 to -52.4 ‰, respectively. The two LMC samples are, in stable isotopic composition rather, similar to the HMC.

5. Discussion

5.1 Methane-related authigenic carbonates

Authigenic carbonates are useful proxies for identifying past and current methane seepage (e.g. Han and Suess, 1989; Hovland et al., 1987; Mazzini et al., 2006; Teichert et al., 2005b; von Rad et al., 1996). In marine sediments, methane is being generated locally or migrating upwards. In the presence of sulfate, methane is anaerobically oxidized (AOM) in the sulphate-methane transition zone (SMTZ). This is also the zone where methane-related authigenic carbonates will form due to the production of bicarbonate and increase in alkalinity. Characteristic low carbon isotope ratios of methane-related carbonates have been identified at Sites 1, 5, 8, 9, 12 and 15 (Fig. 6). At Sites 1, 5, 9 and 12 methane-related carbonates are rather single occurrences while at Sites 8 and 15 they occur abundantly with $\delta^{13}C$ values around -50 ‰. As observed at many other methane seepage locations, the carbonates have a characteristic calcite composition which is high in Mg (10-18 Mol% $MgCO_3$). Methane-related carbonates with similar mineralogy have also been observed in the K-G Basin by Mazumdar et al. (2009) and Teichert et al. (2014).

An important question is if these carbonates are recent precipitates. For Site 8, a previous study (Mazumdar et al., 2009) has shown that carbonates at 16 mbsf have an age of about 46 – 53 ka although the SMTZ is today at this depth. Together with findings of chemosynthetic clams in this depth Mazumdar et al. (2009) conclude that these carbonates represent a paleo methane seep location. Results from this study provide further evidence for carbonate formation near the seafloor. The $CaCO_3$ content of the methane-related carbonates is in the range of 81 – 54 % with a mean of about 70 % (Fig. 7). If we assume that the carbonate has filled completely the free sediment pore space, we may use the $CaCO_3$ content as a first approximation for the depth of carbonate formation. Site 8 is located at approximately the same location as Site 10 (Fig. 1) of the Indian National Gas Hydrate Program (NGHP) Expedition 01 (Collett et al., 2008) and in addition, sediment porosity data of this core has been presented in Mazumdar et al. (2009). The sediment porosity at the seafloor is about 80 % and decreases to 70 % at about 9 mbsf with a minimum of 50 % and less between 16 and 20 mbsf (Mazumdar et al., 2009). This confirms the near-seafloor formation of these methane-related carbonates. The abundant occurrence of carbonates in a depth range from 9 – 28 mbsf might indicate that the SMTZ was quite variable in the past.

For Site 15 we have not further age information on the carbonates but at about 16 mbsf clams have been found. This observation together with a high $CaCO_3$ content (mean: 71 %) also points to carbonate formation near the seafloor and methane seepage.

Bathymetric and multi-channel seismic data has revealed that both locations, Sites 8 and 15, are located on mounds that are associated with fluid and/or gas movement probably related to shale

diapirism (Dewangan et al., 2010). These mounds are similar geologic settings as described at the continental margin of Norway (Hovland, 1990) or the continental slope off Costa Rica (Petersen et al., 2009).

5.2 Fe-rich carbonate formation

Fe-rich carbonates occur abundantly at Sites 2, 5, 6, 9, 11, 12 and 17. Especially at Site 11 they occur almost evenly distributed over a wide depth range of 18 m (Fig. 6). The carbon isotopic composition may help to understand the process of formation of these carbonates. At most locations, the $\delta^{13}C$ values are negative. At Sites 12 and 17 they range between -20 and -10 ‰, at Sites 5 and 6 between -10 and 0 ‰, at Site 10 around 0 ‰ and at Site 11 between 0 and +10 ‰. Site 9 shows a broad range of $\delta^{13}C$ values. The Fe-rich carbonates with heavy, positive carbon isotopic composition have mostly probably been precipitated due to microbial methanogenesis. This process induces authigenic carbonate formation due to an increase in bicarbonate (Claypool and Kaplan, 1974). During methanogenesis, the remaining CO_2 pool in the pore water is successively getting depleted in the light carbon isotope. Therefore, the authigenic carbonates precipitated in this zone often carry a heavy signature between 10 and 20 ‰ (Malone et al., 2002). Pore water geochemical studies at nearby NGHP Expedition 01 Site 10 (Fig. 1) have shown heavy $\delta^{13}C$ values of the dissolved inorganic carbon between 0 and + 10 ‰ below the SMTZ (Solomon et al., 2014).

The carbon isotopic composition of the Fe-rich carbonates with $\delta^{13}C$ values below 0 ‰ cannot be interpreted with absolute certainty. Values around -20 ‰ indicate the process inducing carbonate formation was organoclastic sulphate reduction (OSR) where organic matter is being oxidized. Since the carbon can be a mixture of different sources (marine, terrestrial, dissolved inorganic carbon from seawater), the resulting $\delta^{13}C$ values of the carbonates might also display variable values. It is also possible that due to diffusion, a light carbon isotope ratio from the zone of OSR or AOM may still be present in the zone of methanogenesis. Authigenic carbonates precipitated within the zone of methanogenesis might therefore also show negative display $\delta^{13}C$ values (Malone et al., 2002).

Fe-rich carbonates have often been found within the zone of methanogenesis (Baker and Burns, 1985; Mozley and Carothers, 1992). This is not surprising since Fe is preferentially precipitated as iron sulphide above the SMTZ and usually not available for incorporation into carbonates. Below the SMTZ iron becomes available again and Fe carbonate formation is favored where activities of dissolved sulfide are low and iron and bicarbonate activities are high (Rodriguez et al., 2000).

Supporting evidence for a rather deep formation of the Fe-rich carbonates comes from the $CaCO_3$ content. A mean value of 60.8 % (Fig. 7) can be compared with typical slope basin sediments in the K-G Basin (Site 3, NGHP Expedition 01, Collett et al., 2008) with a $CaCO_3$ content of about 80 % near the seafloor and 60 % in about 40 mbsf. This is however contradicting to the fact that these carbonates have been sampled above 30 mbsf. A possible explanation is the incomplete carbonate cementation of the sediments with Fe-rich carbonates. This will lead to a lower $CaCO_3$ content.

6. Summary and conclusion

1. Methane-related authigenic carbonates with a typical Mg-rich composition (high-Mg calcite) have been identified at Sites 8 and 15. Further evidence like the occurrence of chemosynthetic clams and high calcium carbonate content, indicating carbonate precipitation near the seafloor, indicates that these sites are paleo methane seep locations. The methane flux is probably related to fluid and/or gas movement related to shale diapirism and associated faults. Methane-related carbonates in low abundances have also been identified at Sites 1, 5, 9 and 12.
2. Fe-rich carbonates occur abundantly at many sites in the K-G Basin. Results indicate that they have been precipitated within the zone of organic sulphate reduction and methanogenesis.
3. The high variability of authigenic carbonate mineralogies and carbon isotopic compositions shown in three transects across the K-G Basin indicate that the basin is a highly dynamic biogeochemical system.

Acknowledgements

We thank Directors of CSIR-NIO, CSIR-NGRI, NCAOR, NIOT and secretary MoES, India, for supporting the study, facilities and permission to publish this work. The data used in this study has been acquired with funding from MoES project. H. Leau, head of the Oceanography Department, and P. Sangiardi, in charge of on-board operations of IPEV on board RV Marion Dufresne (MD-161) is thanked for providing on-board technical support and facilities. We thank anonymous reviewers for their thoughtful and constructive reviews. The authors also thank P. Dewangan for preparing the shallow structures and depositional environment map and T. Ramprasad and A. Mazumdar for their valuable inputs. Mr.Girish Prabhu and Mr. Vijay Khedekar are thanked for their help during XRD and SEM operation and data acquisition respectively. This is NIO contribution no XXXX.

References

Baker, P.A., Burns, S.J., 1985. Occurrence and formation of dolomite in organic-rich continental margin sediments. AAPG Bull. 69, 1917-1930.

Claypool, G.E., Kaplan, I.R., 1974. The origin and distribution of methane in marine sediments. In: Kaplan, I.R. (Ed.), Natural Gases in Marine Sediments. Plenum Press, New York, London, 99–139.

Collett, T., Riedel, M., Cochran, J., Boswell, R., Presley, J., Kumar P., Sathe, A., Sethi, A., Lall, M., Sibal, V., 2008. Results of the Indian National Gas Hydrate Program Expedition 01 initial reports, Dir. Gen. of Hydrocarbons, Min. of Pet. and Nat. Gas, New Delhi.

Collett, T.S., Boswell, R., Cochran, J.R., Kumar, P., Lall, M., Mazumdar, A., Ramana, M.V., Ramprasad, T., Riedel, M., Sain, K., Sathe, A.V., Vishwanath, K., NGHP Expedition 01 Scientific Party, 2014. Geologic implications of gas hydrates in the offshore of India: Results of the National Gas Hydrate Program Expedition 01. Mar. Petrol. Geol. 58, 3-28.

Dewangan, P., Ramprasad, T., Ramana, M.V., Mazumdar, A., Desa, M., Badesab, F.K., 2010. Seabed morphology and gas venting features in the continental slope region of Krishna-Godavari basin, bay of bengal: Implications in Gas-Hydrate Exploration. Mar. Petrol. Geol. 27, 1628-1641.

Feng, D., Chen, D. F., Peckmann, J., 2009a. Rare earth elements in seep carbonates as tracers of variable redox conditions at ancient hydrocarbon seeps. Terra Nova 21(1), 49-56.

Feng, D., Chen, D.F., Roberts, H.H., 2009b. Petrographic and geochemical characterization of seep carbonate from Bush Hill (GC 185) gas vent and hydrate site of the Gulf of Mexico. Mar. Petrol. Geol., 26, 1190-1198.

Hovland, M., Talbot, M., Qvale, H., Olausson, S., Aasbeg, L., 1987. Methane-related carbonate cements in pockmarks of the north Sea. J. Sediment. Petrol. 57, 881-892.

Johnson, J.E., Phillips, S.C., Torres, M.E., Piñero, E., Rose, K., Giosan, L., 2014. Influence of total organic carbon deposition on the inventory of gas hydrate in the Indian continental margins. Mar. Petrol. Geol. 58, 406-424.

Klauda, J.B., Sandler, S.I., 2005. Global distribution of methane hydrate in ocean sediment. Energ. Fuel. 19, 459-470.

Kocherla, M., Mazumdar, A., Karisiddaiah, S.M., Borole D.V. and Rao, B.R., 2006. Evidences of methane derived authigenic carbonates from the sediments of the Krishna – Godavari Basin, eastern continental margin of India. Curr. Sci. India 91, 318-323.

Kumar, P., Collett, T.S., Boswell, R., Cochran, J.R., Lall, M., Mazumdar, A., Ramana, M.V., Ramprasad, T., Riedel, M., Sain, K., Sathe, A.V., Vishwanath, K., Yadav, U.S., NGHP Expedition 01 Scientific Party, 2014. Geologic implications of gas hydrates in the offshore of India: Krishna-Godavari Basin, Mahanadi Basin, Andaman Sea, Kerala-Konkan Basin. Mar. Petrol. Geol. 58, 29-98.

Lumsden, D.S., 1979. Discrepancy between thin-section and x-ray estimates of dolomite in limestone. J. Sed. Petrol. 49, 429–436.

Mazumdar, A., Joao, H. M., Peketi, A., Dewangan, P., Kocherla, M., Joshi, R.K., Ramprasad, T., 2012. Geochemical and geological constraints on the composition of marine sediment pore fluid: Possible link to gas hydrate deposits. Mar. Petrol. Geol. 38, 35-52.

Mazumdar A., Dewangan, P., Joa¨o, H.M., Peketi, A., Khosla, V.R., Kocherla, M., Badesab, F.K., Joshi, R.K., Roxanne, P., Ramamurty, P.B., Karisiddaiah., S.M., Patil, D.J., Dayal, A.M., Ramprasad, T., Hawkesworth, C.J., Avanzinelli, R., 2009. Evidence of paleo–cold seep activity from the Bay of Bengal, offshore India. Geochem. Geophy. Geosy. 10, 1-15.

Mazzini, A., Svensen, H., Hovland, M., Planke, S., 2006. Comparison and implications from strikingly different authigenic carbonates in a Nyegga complex pockmark, G11, Norwegian Seas. Mar. Geol. 231, 89-102.

Mozley, P.S., Carothers, W.W. 1992. Elemental and isotopic composition of siderite in the Kuparuk formation, Alaska: effect of microbial activity and water/sediment interaction on early pore-water chemistry. J. Sediment. Petrol. 62, 681-692.

Naehr, T.H., Eichhubl, P., Orphan, V.J., Hovland, M., Paull, C.K., Ussler III, W., Lorenson, T.D., Greene, H.G., 2007. Authigenic carbonate formation at hydrocarbon seeps in continental margin sediments: A comparative study. Deep Sea Res. II 54, 1268-1291.

Ojha, P.S., Dubey, M., 2006. Giant hydrocarbons fields of offshore Krishna-Godavari basin, Petroview 1. Directorate General of Hydrocarbons, New Delhi, 26–30.

Peckmann, J., Daniel, B., Steffen, K., 2009. Molecular fossils reveal fluid composition and flow intensity at a Cretaceous. Geology 37, 847-850.

Petersen, C., Klaucke, I., Weinrebe, W., Ranero, C., 2009. Fluid seepage and mound formation offshore Costa Rica revealed by deep-towed sidescan sonar and subbottom profiler data. Mar. Geol. 266, 172-181.

Phillips, S.C., Johnson, J.E., Underwood, M.B., Guo J., Giosan, L., Rose, K., 2014. Long-timescale variation in bulk and clay mineral composition of Indian continental margin sediments in the Bay of Bengal, Arabian Sea, and Andaman Sea. Mar. Petrol. Geol. 58, 117-138.

Prabhakar, K.N., Zutshi, P.L., 1993. Evolution of southern part of Indian east coast basins. J. Geol. Soc. India 41, 215-230.

Ramana, M.V., Nair, R.R., Sarma, K.V.L.N.S., Ramprasad, T., Krishnaa, K.S., Subrahmanyam, V., D'Cruza, M., Subrahmanyam, C., Paul, J., Subrahmanyam, V. D., Chandra Sekhar, V., 1994. Mesozoic anomalies in the Bay of Bengal. Earth Planet. Sci. Lett. 121, 469–475.

Ramana, M.V, Ramprasad, T., Kamesh Raju, K.A., Desa, M., 2007. Occurrence of gas hydrates along the continental margins of India, particularly the Krishna-Godavari offshore basin. Int. J. Environ. Stud. 64, 675-693.

Ramana, M.V, Ramprasad, T., Paropkar A.L, Borolei, D.V. Ramalingeswara Rao B., Karisiddaiah, S.M., Desa, M., Kocherla, M., Joao, H.M., Lokabharati .P., Gonsalves., Pattan, M.-J., J.N., Khadge, N.H., Prakash Babu, C., Sathe, A.V., Kumar, P., Sethi, A.K., 2009. Multidisciplinary investigations exploring indicators of gas hydrate occurrence in the Krishna–Godavari Basin offshore, east coast of India. Geo-Mar. Lett. 29, 25-38.

Ramprasad, T., Dewangan, P., Ramana, M.V., Mazumdar, A., Karisiddaiah, S.M., Ramya, E.R., Sriram, G., 2011. Evidence of slumping/sliding in Krishna-Godavari offshore basin due to gas/fluid movements. Mar. Petrol. Geol. 28,1806-1816.

Rao, G.N., 2001. Sedimentation, stratigraphy, and petroleum potential of Krishna-Godavari Basin, East Coast of India. AAPG Bull. 85, 1623-1643.

Rodriguez, N.M., Paull, C.K., Borowski, W.S., 1999. Zonation of authigenic carbonates within gas hydrate-bearing sedimentary sections on the Blake Ridge: Offshore Southeastern North America. In: Paull, C.K., Matsumoto, R., Wallace, P.J., and Dillon, W.P. (Eds.), Proc. ODP, Sci. Results 164, College Station, TX (Ocean Drilling Program), 29-36.

Scotese, C.R., Gahagan, L.M., Larson, R.L., 1988. Plate tectonic reconstructions of the Cretaceous and Cenozoic ocean basins. Tectonophysics 155, 27-48.

Solomon, E.A., Spivack, A.J., Kastner, M., Torres, M.E., Robertson, G., 2014. Gas hydrate distribution and carbon sequestration through coupled microbial methanogenesis and silicate weathering in the Krishna-Godavari basin, offshore India. Mar. Petrol. Geol. 58, 233-253

Suess, E., 2014. Marine cold seeps and their manifestations: geological control, biogeochemical criteria and environmental conditions. Int. J. Earth Sci. 103, 1889-1916.

Teichert, B.M.A., Eisenhauer, A., Bohrmann, G., Haase-Schramm, A., Bock, B., Linke, P., 2003. U/Th systematics and ages of authigenic carbonates from Hydrate Ridge, Cascadia Margin: recorders of fluid flow variations. Geochim. Cosmochim Ac. 67, 3845–3857.

Teichert, B.M.A., Bohrmann, G., 2005a. Data report: Composition of authigenic carbonates in sediments of the Cascadia accretionary prism, ODP Leg 204. In Tréhu, A.M., Bohrmann, G., Torres, M.E., and Colwell, F.S. (Eds.), Proc. ODP, Sci. Results, 204, 1–8.

Teichert, B.M.A., Bohrmann, G., Suess, E., 2005b. Chemoherms on Hydrate Ridge - Unique microbially-mediated carbonate build-ups growing into the water column. Palaeogeogr. Palaeocl., 227, 67-85.

Teichert, B.M.A., Johnson, J.E., Solomon, E.A., Giosan, L., Rose, K., Kocherla, M., Connolly, E.C., Torres, M.E., 2014. Composition and origin of authigenic carbonates in the Krishna-Godavari and Mahanadi Basins, eastern continental margin of India. Mar. Petrol. Geol. 58, 438-460.

von Rad U., Roesch, H., Berner, U., Geyh, M., Marchig, V., Schulz, H., 1996. Authigenic carbonates derived from oxidized methane vented from the Makran accretionary prism off Pakistan. Mar. Geol. 136, 55-77.

Figure Captions

Figure 1
Bathymetric map showing shallow structures and depositional environment information in the K-G offshore basin from Dewangan et al. (2010). Inset delineates the location of the K-G basin. Core locations of R/V *Marion Dufresne* cruise M-161 are indicated by blue circles and labeled with 'M'. Cores drilled by R/V JOIDES Resolution during NGHP-01 expediton are labelled with 'J'.

Figure 2
Depth distribution (meters below seafloor) of all sampled authigenic carbonates with respect to water depth of core locations. Core sites are shown as numbers.

Figure 3
Morphology of authigenic carbonate samples: (A) tube, Site 15, 29.02 mbsf; (B) tubes, HMC, Site 8, 17.52 mbsf; (C) nodule with tube, Site 15, 29.02 mbsf; (D) nodule, Site 9, 8.80 mbsf; (E) semi-lithified Fe-rich carbonate nodule, Site 9, 16.25 mbsf; (F) semi-lithified Fe-rich carbonate nodule, Site 12, 22.25 mbsf. Scale bar is 1 cm.

Figure 4
SEM micrographs: (a, b) porous fabric on the surface of a Fe-rich carbonate, probably due to gaseous sediments; (c, d) euhedral micro-crystalline texture of Fe-rich carbonate; (e, f) occurrence of pyrite framboids.

Figure 5
Oxygen and carbon isotopic composition of LMC, HMC and Fe-rich carbonates from all sites.

Figure 6
Carbon isotopic composition with depth (mbsf) of Sites 1, 5, 6, 8, 9, 10, 11, 12, 15 and 17 in three NNW-SSE trending profiles across the K-G Basin. Total distance between sites of each profile are given in kilometres. Stippled line indicates depth of the SMTZ after Mazumdar et al. (2012). Vertical grey line is a visual orientation to differentiate between organic carbon as carbon source for carbonates (> -25 ‰) and methane as carbon source (< -25 ‰).

Figure 7
Carbon isotopic composition versus calcium carbonate content (wt. %) of authigenic carbonate samples of all studied sites. Light gray diamonds are LMC and HMC samples, dark gray diamonds are Fe-rich carbonate samples. Shaded areas depict methane-derived carbonates (light grey) and other authigenic carbonates (dark grey). The mean value of calcium carbonate content is given for each group of carbonates.

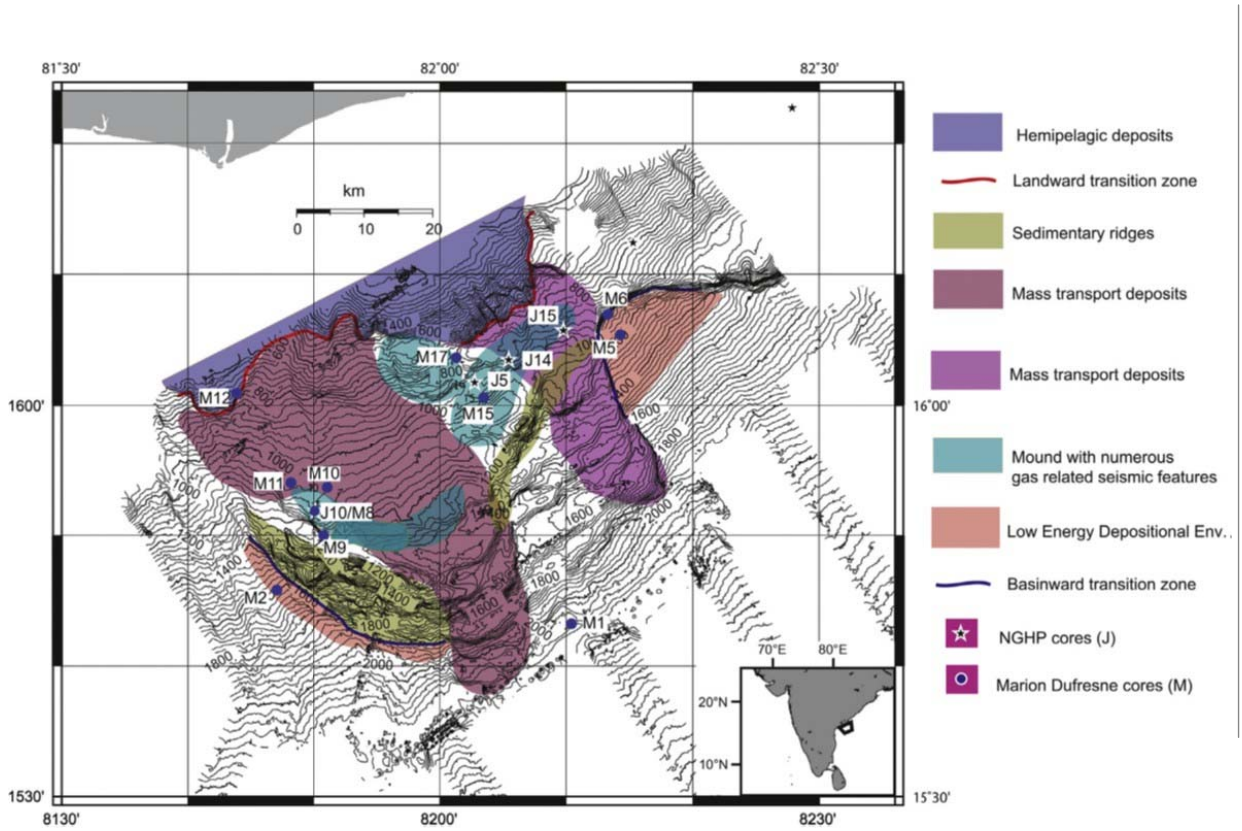

Figure1
Kocherla et al.

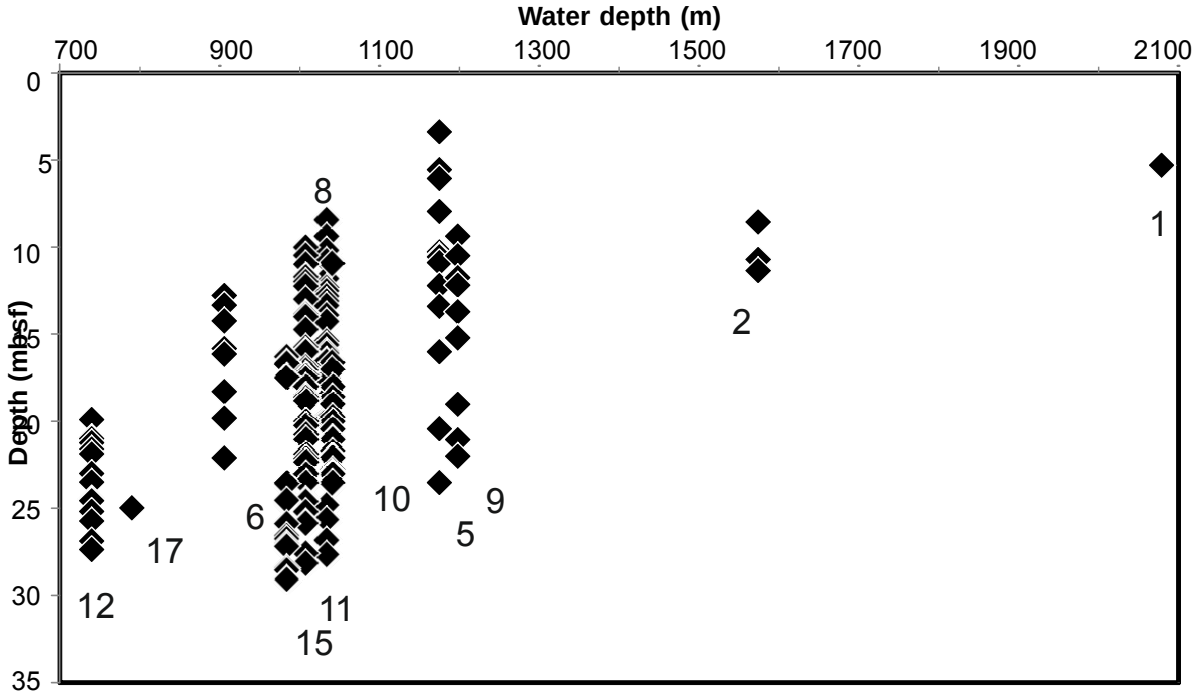

Figure 2
Kocherla et al.

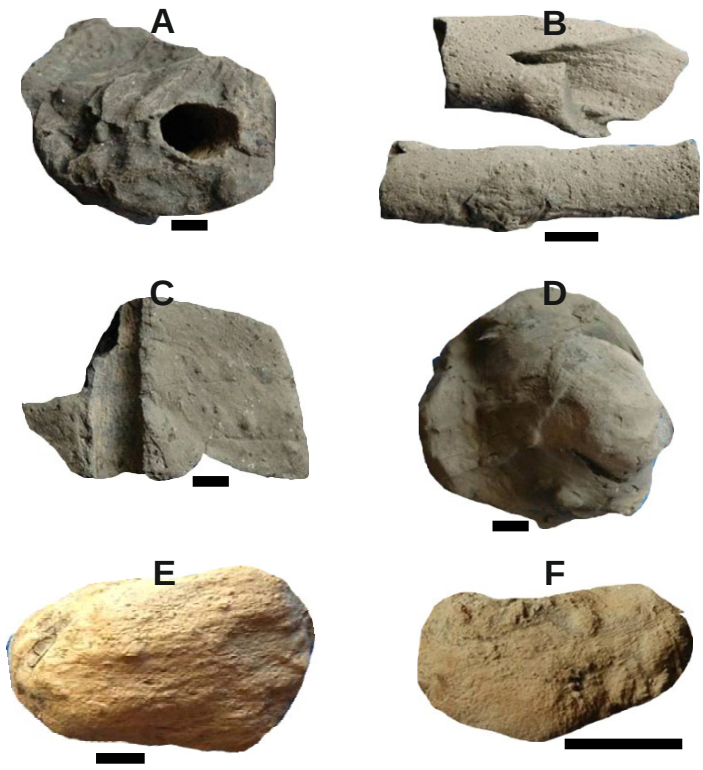

Figure 3 Kocherla et al.

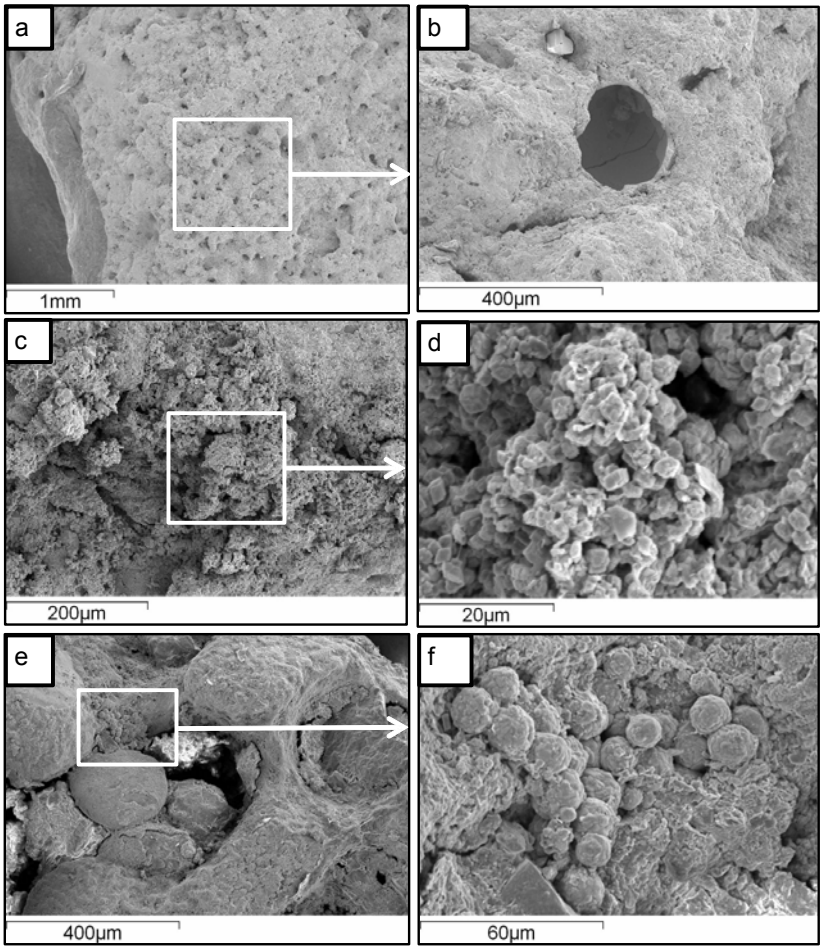

Figure 4 Kocherla et al.

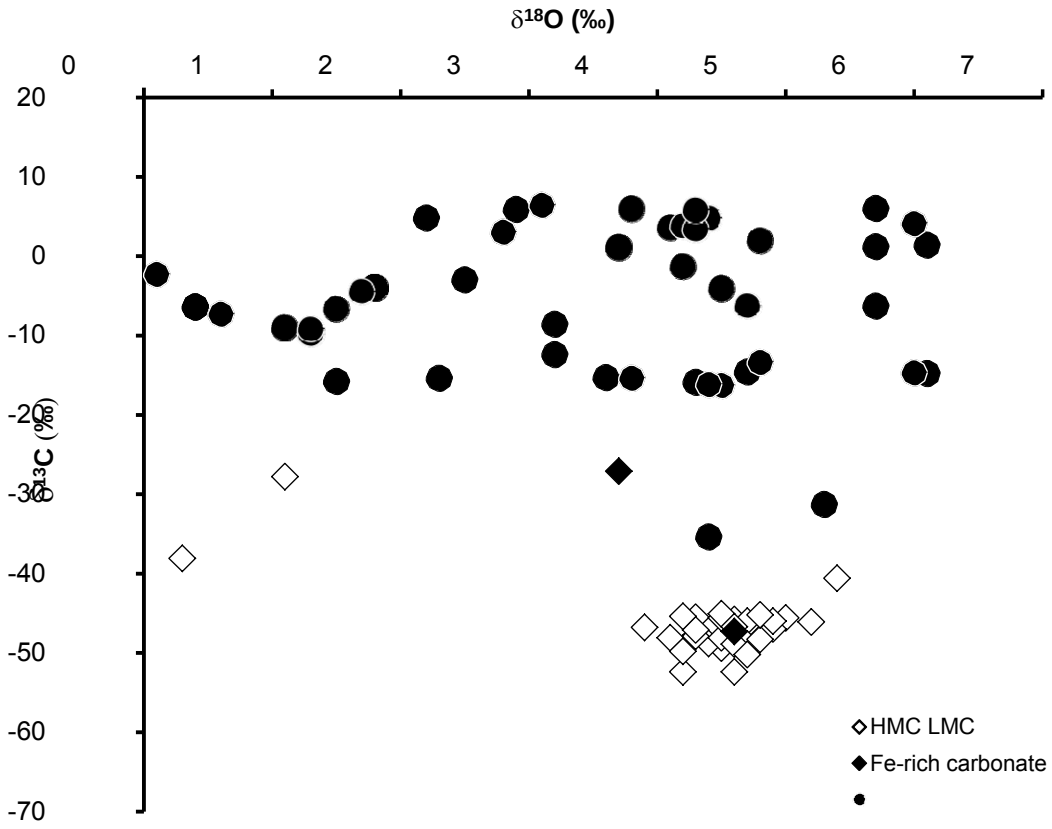

Figure 5 Kocherla et al.

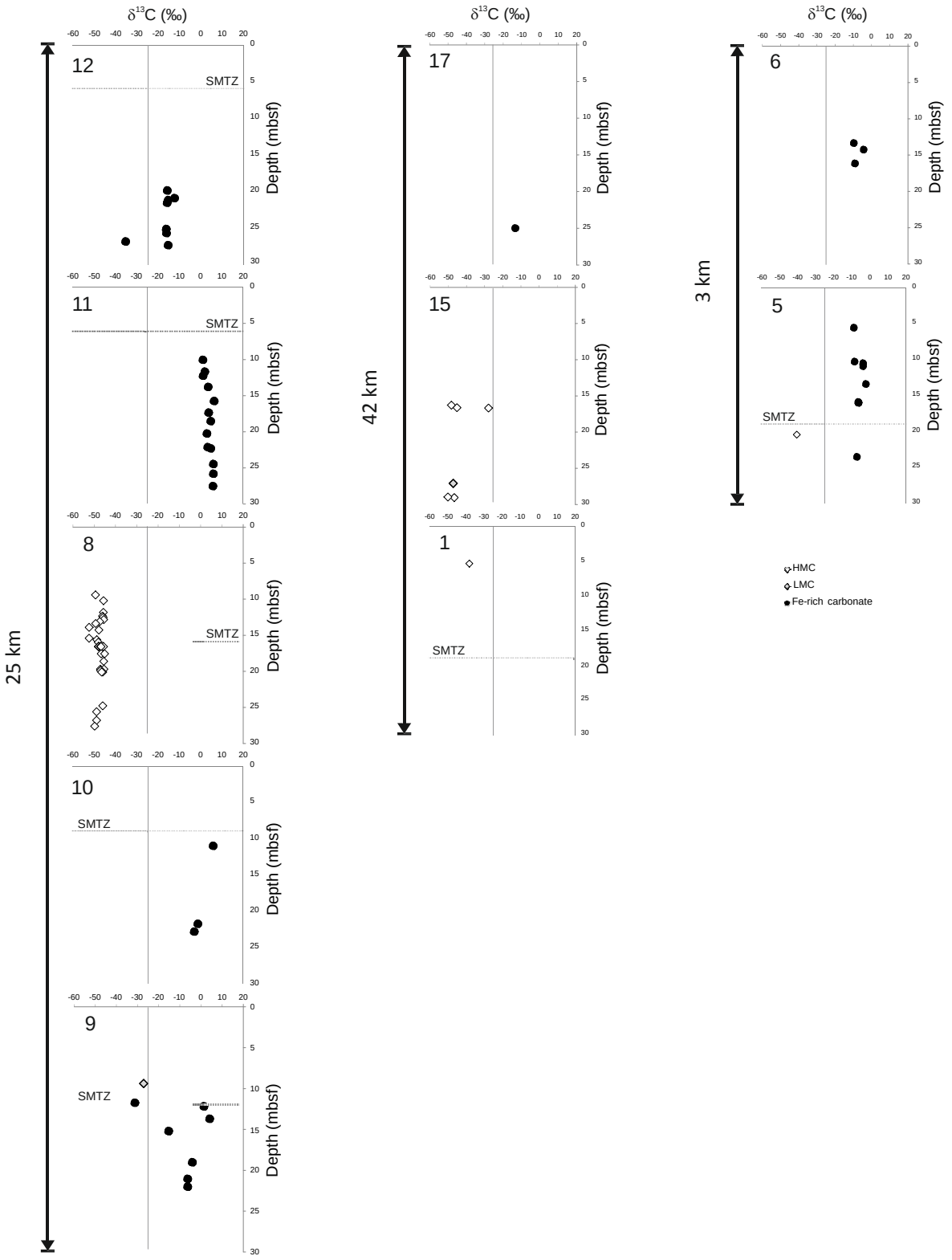

Figure 6

Kocherla et al.

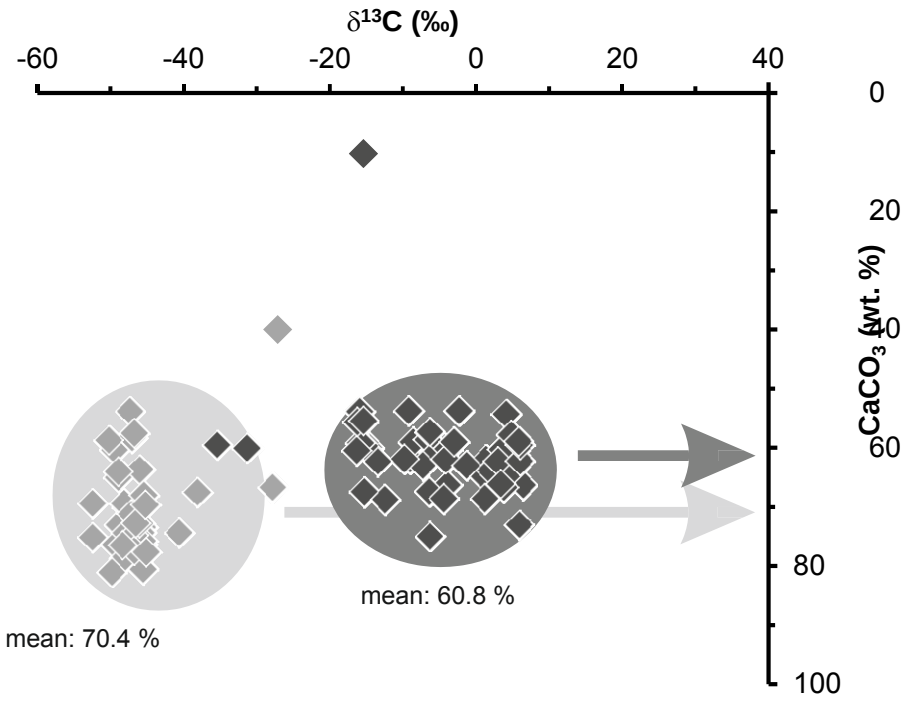

Figure-7
Kocherla et al

Table 1

Locations, water depth, core length, sulfate—methane transition zone (SMTZ) of sediment cores from R/V *Marion Dufresne* cruise MD-161.

Site	Latitude N	Longitude E	Water depth (m)	Core length (m)	Approx. SMTZ depth (m)
17	16 03.6300 N	82 01.2900 E	790	30.0	24.9
18	17 26.3106 N	83 49.9501 E	1691	32.0	12
19	18 59.1092 N	85 41.1669 E	1480	39.1	11.21
20	18 47.3600 N	85 36.4400 E	1866	50.1	17.17
21	19 05.3872 N	85 35.9960 E	986	36.4	19.65
22	19 09.0000 N	85 46.3900 E	1365	32.4	15
23	19 06.2500 N	85 50.1500 E	1600	38.6	17.25
24	19 03.4825 N	85 45.8415 E	1578	31.9	16.89
25	19 01.8100 N	85 38.3498 E	1429	39.2	24.06
26	19 13.9900 N	85 37.4699 E	414	34.2	11.21
27	18 57.3600 N	85 43.4400 E	1691	36.1	18.62

[a] Based on pore water geochemistry by Mazumdar et al. (2009).

Table 2
Mineralogy and stable isotope data of cores from R/V *Marion Dufresne* cruise MD-161.

Site	Sample depth (m)	Color	Appearance	Type	Main carbonate mineral	Mol% $MgCO_3$	$CaCO_3$ (wt %)	$5^{13}C$ (‰ PDB)	$\delta^{18}O$(‰ PDB)
1	5.31	gray	semi-lithified	micro nodule	HMC	14.5	67.5	-38.1	0.3
2	8.56	brown	semi-lithified	micro nodule	Fe-rich carbonate		60.0	-14.6	4.7
	10.72	brown	lithified	nodule	Fe-rich carbonate		60.3	-14.8	6.1
	11.36	brown	lithified	nodule	Fe-rich carbonate		60.4	-14.7	6.0
5	3.39	yellow	semi-lithified	micro nodule	Fe-rich carbonate		54.3		
	5.56	yellow	semi-lithified	nodule	Fe-rich carbonate		61.9	-9.0	1.1
	6.07	brown	semi-lithified	micro nodule	Fe-rich carbonate		54.3		
	7.96	brown	semi-lithified	micro nodule	Fe-rich carbonate		67.4		
	10.28	yellow	semi-lithified	nodule	Fe-rich carbonate		59.1	-8.6	3.2
	10.51	brown	semi-lithified	nodule	Fe-rich carbonate		60.1	-3.9	1.8
	10.56	brown	semi-lithified	nodule	Fe-rich carbonate		60.3	-3.9	1.8
	10.91	brown	semi-lithified	nodule	Fe-rich carbonate		66.3	-3.9	1.8
	12.22	brown	semi-lithified	nodule	Fe-rich carbonate		66.8		
	13.40	brown	semi-lithified	nodule	Fe-rich carbonate		53.8	-2.3	0.1
	15.90	brown	semi-lithified	nodule	Fe-rich carbonate		58.7	-6.6	1.5
	15.95	brown	semi-lithified	nodule	Fe-rich carbonate		57.5	-6.4	0.4
	16.00	brown	semi-lithified	nodule	Fe-rich carbonate		67.4	-6.4	0.4
	16.02	brown	semi-lithified	nodule	Fe-rich carbonate		61.9	-6.4	0.4
	20.43	gray	lithified	tube	HMC	12.5	74.3	-40.6	5.4
	23.53	brown	semi-lithified	nodule	Fe-rich carbonate		63.0	-7.3	0.6
6	12.78	brown	semi-lithified	micro nodule	Fe-rich carbonate				
	13.34	brown	semi-lithified	nodule	Fe-rich carbonate		61.9	-9.8	1.3
	14.24	brown	semi-lithified	nodule	Fe-rich carbonate		68.6	-4.4	1.7
	15.82	brown	semi-lithified	nodule	Fe-rich carbonate				
	16.15	yellow	semi-lithified	micro nodule	Fe-rich carbonate		53.8	-9.2	1.3
	18.32	yellow	semi-lithified	micro nodule	Fe-rich carbonate				
	19.83	yellow	semi-lithified	micro nodule	Fe-rich carbonate				
	22.11	brown	semi-lithified	micro nodule	Fe-rich carbonate				
8	8.48	gray	semi-lithified	micro nodule	HMC				
	9.41	gray	semi-lithified	micro nodule	HMC	16.1	60.3	-49.4	4.5
	10.21	gray	semi-lithified	tube	HMC	17.7	73.4	-45.6	5.0
	10.81	gray	semi-lithified	nodule	HMC	18.1			
	11.82	gray	semi-lithified	tube	HMC	18.1	76.3	-45.7	4.8
	12.34	gray	lithified	tube	HMC	18.1	73.8	-46.1	5.2
	12.53	gray	lithified	tube	HMC	17.7	74.3	-45.8	4.6
	12.83	gray	lithified	tube	HMC	17.1	80.6	-45.5	4.3
	13.11	gray	lithified	tube	HMC	17.1	74.9	-47.4	4.6
	13.37	gray	lithified	tube	HMC	18.4	76.4	-49.3	4.7
	13.9	gray	lithified	tube	HMC	15.1	69.4	-52.4	4.6
	14.27	gray	lithified	nodule	HMC	17.4	70.1	-47.8	4.3
	15.41	gray	lithified	tube	HMC	18.4	75.2	-52.4	4.2
	15.61	gray	lithified	tube	HMC	15.8	73.0	-48.8	4.4
	15.97	gray	semi-lithified	nodule	HMC	15.1	69.4	-48.1	4.1
	16.10	gray	semi-lithified	tube	HMC				
	16.50	gray	semi-lithified	tube	HMC	15.8			
	16.52	gray	semi-lithified	tube	HMC	14.2			
	16.56	gray	semi-lithified	tube	HMC	9.3			
	16.56	gray	semi-lithified	tube	HMC	12.4	78.7	-48.1	4.5
	16.56	gray	semi-lithified	tube	HMC	12.4	74.4	-47.9	4.3
	16.56	gray	semi-lithified	tube	HMC	12.6	75.8	-45.6	4.5
	16.56	gray	semi-lithified	tube	HMC	12.4	76.3	-47.1	4.3
	16.56	gray	semi-lithified	tube	HMC	12.4	74.8	-46.8	3.9
	17.52	gray	semi-lithified	tube	HMC	15.1			
	17.56	gray	semi-lithified	tube	HMC	12.8	77.4	-46.7	4.7
	17.56	gray	semi-lithified	tube	HMC	12.4	77.7	-45.1	4.5
	18.61	gray	semi-lithified	micro nodule	HMC	12.9	70.0	-45.5	4.8
	18.63	gray	semi-lithified	micro nodule	HMC	9.9			
	19.62	gray	semi-lithified	micro nodule	HMC	12.2			
	19.65	gray	semi-lithified	micro nodule	HMC	13.5			
	19.70	gray	semi-lithified	micro nodule	HMC	12.4	71.3	-47.1	4.7
	19.70	gray	semi-lithified	micro nodule	HMC	12.7	68.0	-45.4	4.2
	19.80	gray	lithified	micro nodule	HMC				
	19.89	gray	semi-lithified	micro nodule	HMC	11.5	58.3	-47.0	4.9
	20.11	gray	semi-lithified	nodule	HMC	12.6	72.8	-46.0	4.9
	20.11	gray	semi-lithified	nodule	HMC	12.8	72.8	-46.5	4.7
	20.13	gray	semi-lithified	nodule	HMC	11.2			
	24.78	gray	semi-lithified	micro nodule	HMC	12.9	63.7	-46.0	4.7
	25.61	gray	semi-lithified	micro nodule	HMC	12.5	65.0	-48.9	4.7
	26.79	gray	semi-lithified	micro nodule	HMC	12.9	64.0	-48.9	4.6
	27.60	gray	semi-lithified	micro nodule	HMC	9.9	81.1	-49.8	4.2
9	9.38	gray	lithified	nodule	LMC	5.3	40.0	-27.1	3.7
	10.50	brown	semi-lithified	nodule	Fe-rich carbonate				
	11.75	brown	semi-lithified	nodule	Fe-rich carbonate		60.0	-31.3	5.3

{continued on next page)

Table 2 *(continued)*

Site	Sample depth (m)	Color	Appearance	Type	Main carbonate mineral	Mol% $MgCO_3$	$CaCO_3$ (wt %)	$\delta^{13}C$ (‰ PDB)	$\delta^{18}O$ (‰ PDB)
	12.19	brown	semi-lithified	nodule	Fe-rich carbonate		62.0	1.4	6.1
	13.71	brown	semi-lithified	nodule	Fe-rich carbonate		54.3	4.1	6.0
	15.22	brown	semi-lithified	nodule	Fe-rich carbonate		67.5	-15.3	3.6
	19.03	brown	semi-lithified	nodule	Fe-rich carbonate		62.0	-4.1	4.5
	21.06	brown	semi-lithified	nodule	Fe-rich carbonate		75.0	-6.3	4.7
	22.02	brown	semi-lithified	nodule	Fe-rich carbonate		57.3	-6.3	5.7
10	10.96	brown	semi-lithified	micro nodule	Fe-rich carbonate		73.0	5.9	2.9
	16.61	brown	semi-lithified	micro nodule	Fe-rich carbonate				
	17.00	brown	semi-lithified	micro nodule	Fe-rich carbonate				
	18.00	brown	semi-lithified	micro nodule	Fe-rich carbonate				
	18.61	brown	semi-lithified	micro nodule	Fe-rich carbonate				
	19.00	brown	semi-lithified	micro nodule	Fe-rich carbonate				
	19.73	brown	semi-lithified	micro nodule	Fe-rich carbonate				
	20.00	brown	semi-lithified	micro nodule	Fe-rich carbonate				
	20.42	brown	semi-lithified	micro nodule	Fe-rich carbonate				
	20.94	brown	semi-lithified	micro nodule	Fe-rich carbonate				
	21.00	brown	semi-lithified	micro nodule	Fe-rich carbonate				
	21.69	brown	semi-lithified	nodule	Fe-rich carbonate		63.0	-1.3	4.2
	22.00	brown	semi-lithified	nodule	Fe-rich carbonate				
	22.07	brown	semi-lithified	nodule	Fe-rich carbonate				
	22.77	brown	semi-lithified	nodule	Fe-rich carbonate		59.1	-3.0	2.5
	22.91	brown	semi-lithified	nodule	Fe-rich carbonate				
	22.96	brown	semi-lithified	nodule	Fe-rich carbonate				
	23.00	brown	semi-lithified	micro nodule	Fe-rich carbonate				
	23.50	brown	semi-lithified	micro nodule	Fe-rich carbonate				
11	10.04	brown	semi-lithified	nodule	Fe-rich carbonate		64.9	1.1	3.7
	10.50	brown	semi-lithified	nodule	Fe-rich carbonate				
	11.00	brown	semi-lithified	nodule	Fe-rich carbonate				
	11.68	brown	semi-lithified	nodule	Fe-rich carbonate		63.8	2.0	4.8
	11.73	brown	semi-lithified	nodule	Fe-rich carbonate				
	12.00	brown	semi-lithified	nodule	Fe-rich carbonate				
	12.25	brown	semi-lithified	nodule	Fe-rich carbonate		68.6	1.2	5.7
	13.00	brown	semi-lithified	nodule	Fe-rich carbonate				
	13.80	brown	semi-lithified	nodule	Fe-rich carbonate		60.3	3.6	4.1
	13.86	brown	semi-lithified	nodule	Fe-rich carbonate				
	14.00	brown	semi-lithified	nodule	Fe-rich carbonate				
	14.73	brown	semi-lithified	nodule	Fe-rich carbonate				
	15.75	brown	semi-lithified	micro nodule	Fe-rich carbonate		66.3	6.4	3.1
	15.95	brown	semi-lithified	nodule	Fe-rich carbonate				
	16.00	brown	semi-lithified	nodule	Fe-rich carbonate				
	16.88	brown	semi-lithified	nodule	Fe-rich carbonate				
	17.06	brown	semi-lithified	nodule	Fe-rich carbonate				
	17.30	brown	semi-lithified	nodule	Fe-rich carbonate				
	17.36	brown	semi-lithified	nodule	Fe-rich carbonate		66.8	3.8	4.2
	17.52	brown	semi-lithified	nodule	Fe-rich carbonate				
	18.00	brown	semi-lithified	nodule	Fe-rich carbonate				
	18.53	brown	semi-lithified	nodule	Fe-rich carbonate		64.0	4.8	4.4
	18.64	brown	semi-lithified	nodule	Fe-rich carbonate				
	18.83	brown	semi-lithified	nodule	Fe-rich carbonate				
	20.00	brown	semi-lithified	nodule	Fe-rich carbonate				
	20.24	brown	semi-lithified	nodule	Fe-rich carbonate		62.3	3.0	2.8
	20.74	brown	semi-lithified	nodule	Fe-rich carbonate				
	21.00	brown	semi-lithified	nodule	Fe-rich carbonate				
	21.89	brown	semi-lithified	nodule	Fe-rich carbonate				
	22.13	brown	semi-lithified	nodule	Fe-rich carbonate		66.2	3.4	4.3
	22.31	brown	semi-lithified	nodule	Fe-rich carbonate		57.8	4.8	2.2
	23.00	brown	semi-lithified	nodule	Fe-rich carbonate				
	23.50	brown	semi-lithified	nodule	Fe-rich carbonate				
	24.47	brown	semi-lithified	nodule	Fe-rich carbonate		62.3	6.0	5.7
	24.53	brown	semi-lithified	nodule	Fe-rich carbonate				
	24.58	brown	semi-lithified	nodule	Fe-rich carbonate				
	25.15	brown	semi-lithified	nodule	Fe-rich carbonate				
	25.75	brown	semi-lithified	nodule	Fe-rich carbonate				
	25.82	brown	semi-lithified	nodule	Fe-rich carbonate		59.6	6.0	3.8
	27.53	brown	semi-lithified	nodule	Fe-rich carbonate		59.0	5.8	4.3
	28.10	brown	semi-lithified	nodule	Fe-rich carbonate				
12	19.91	brown	semi-lithified	nodule	Fe-rich carbonate		59.3	-15.8	1.5
	20.94	brown	semi-lithified	nodule	Fe-rich carbonate		68.8	-12.4	3.2
	21.00	brown	semi-lithified	nodule	Fe-rich carbonate				
	21.23	brown	semi-lithified	nodule	Fe-rich carbonate		10.3	-15.4	3.8
	21.60	brown	semi-lithified	tube	Fe-rich carbonate		53.9	-15.9	4.3
	21.89	brown	semi-lithified	nodule	Fe-rich carbonate				
	23.00	brown	semi-lithified	nodule	Fe-rich carbonate				
	23.50	brown	semi-lithified	nodule	Fe-rich carbonate				
	24.47	brown	semi-lithified	nodule	Fe-rich carbonate				

Table 2 (*continued)*

Site	Sample depth (m)	Color	Appearance	Type	Main carbonate mineral	Mol% $MgCO_3$	$CaCO_3$ (wt %)	$\delta^{13}C$ (‰ PDB)	$\delta^{18}O$ (‰ PDB)
	24.53	brown	semi-lithified	nodule	Fe-rich carbonate				
	24.58	brown	semi-lithified	nodule	Fe-rich carbonate				
	25.18	brown	semi-lithified	nodule	Fe-rich carbonate		60.5	-16.3	4.5
	25.74	brown	semi-lithified	nodule	Fe-rich carbonate		55.7	-16.2	4.4
	26.89	brown	semi-lithified	nodule	Fe-rich carbonate		59.5	-35.4	4.4
	27.38	brown	semi-lithified	nodule	Fe-rich carbonate		55.5	-15.4	2.3
15	16.29	gray	semi-lithified	micro nodule	HMC	10.2	76.5	-48.3	4.8
	16.61	gray	semi-lithified	micro nodule	HMC	15.5	69.7	-45.2	4.8
	16.66	gray	semi-lithified	micro nodule	HMC	18.1	66.7	-27.8	1.1
	17.41	gray	semi-lithified	micro nodule	calcite				
	17.47	gray	semi-lithified	micro nodule	calcite				
	23.54	gray	semi-lithified	micro nodule	calcite				
	24.57	gray	semi-lithified	micro nodule	calcite				
	24.50	gray	semi-lithified	micro nodule	calcite				
	25.85	gray	semi-lithified	micro nodule	calcite				
	26.53	gray	semi-lithified	micro nodule	calcite				
	26.71	gray	semi-lithified	micro nodule	calcite				
	27.00	gray	semi-lithified	micro nodule	calcite				
	27.11	gray	semi-lithified	micro nodule	LMC	6.3	53.8	-47.3	4.6
	27.14	gray	semi-lithified	micro nodule	calcite				
	28.38	gray	semi-lithified	micro nodule	calcite				
	28.50	gray	semi-lithified	micro nodule	calcite				
	28.98	gray	semi-lithified	nodule	HMC	10.9	58.7	-50.2	4.7
	29.03	gray	semi-lithified	nodule	HMC	12.5	57.5	-46.7	4.6
17	24.98	brown	semi-lithified	micro nodule	Fe-rich carbonate		62.3	-13.4	4.8